A tale of two domes: Neogene to recent volcanism and dynamic uplift of northeast Brazil and southwest Africa

M. Klöcking[a,b], M.J. Hoggard[c,d], V. Rodríguez Tribaldos[e], F.D. Richards[d,f], A.R. Guimarães[g], J. Maclennan[a], N.J. White[a]

[a] *Bullard Laboratories, Department of Earth Sciences, University of Cambridge, UK*
[b] *Research School of Earth Sciences, The Australian National University, Acton, ACT, Australia*
[c] *Lamont-Doherty Earth Observatory, Columbia University, New York, USA*
[d] *Department of Earth and Planetary Sciences, Harvard University, Cambridge, MA, USA*
[e] *Lawrence Berkeley National Laboratory, Berkeley, CA, USA*
[f] *Department of Earth Science and Engineering, Imperial College London, UK*
[g] *School of GeoSciences, University of Edinburgh, UK*

Abstract

Topographic domes that are distant from active plate boundaries are often characterised by rapid, youthful uplift, contemporaneous mafic volcanism, radial drainage patterns, and positive long-wavelength gravity anomalies. There is increasing evidence that they are underlain by anomalously low sub-plate seismic velocities. Despite their well-known geomorphological expression, the origin of these epeirogenic features remains enigmatic and is much debated. Here, we investigate potential mechanisms for rapid regional uplift by combining disparate observations from the Borborema and Angolan plateaux that straddle the Brazilian and southwest African margins, respectively. Oceanic residual depth measurements, drainage analysis, stratigraphic architecture, emergent marine terraces and basement denudation are used to constrain their regional uplift histories. In both cases, the bulk of topographic growth occurred within the last 30 Ma in the absence of significant tectonic deformation. We estimate present-day mantle temperature and lithospheric thickness from Neogene to recent volcanic trace element compositions and upper mantle shear wave velocities. Volcanic geochemistry in northeast Brazil is compatible with decompression melting of warm asthenosphere and potentially a minor contribution from metasomatised lithospheric mantle. In Angola, melting of metasomatised lithosphere is probably triggered by injection of small-degree asthenospheric-derived melts. We find no evidence for an asthenospheric thermal anomaly > 50°C above ambient beneath either region. Present-day lithospheric thickness is ~ 100 km beneath Angola and could be as thin as 60 km in the Borborema Province. For Angola, thermobarometry on mantle xenocrysts from Cretaceous kimberlites is used to estimate palaeogeothermal gradients. Results indicate a pre-existing gradient in lithospheric thickness between the edge of the Congo craton and the centre of the Angolan dome at ~ 120 Ma. This gradient likely steepened as a result of additional Neogene thinning by 30 ± 10 km beneath the centre of the dome. We conclude that the mechanism for Neogene epeirogenic uplift of the Borborema and Angolan domes is introduction of a small positive temperature anomaly into the asthenosphere that

causes thermomechanical thinning of the overlying lithospheric mantle.

Keywords: dynamic topography, landscape evolution, intraplate magmatism, xenolith thermobarometry, asthenospheric temperature, lithospheric structure,

1. Introduction

It is widely accepted that most of Earth's topography is isostatically supported by variations in both thickness and density of lithospheric plates. Nonetheless, it is increasingly recognised that a significant additional component of topography that varies through space and time is generated by convection of the underlying mantle (e.g. Gurnis et al., 2000; Moucha et al., 2008; Hoggard et al., 2016; Davies et al., 2019). This dynamic topography is particularly well expressed on the African continent, where $\sim$ 1000 km wide basins and swells have developed since Cretaceous times in locations far from active plate boundaries (Sahagian, 1988; Burke and Gunnell, 2008; Colli et al., 2014). Many similar domes have been described in both continental and oceanic settings. They typically have diameters of up to 2000 km and amplitudes of 1–2 km. Many have approximately circular planforms and semi-radial drainage patterns when they are sub-aerially exposed. Other common features include positive long-wavelength free-air gravity anomalies, coincident low shear-wave velocity anomalies in the underlying mantle, mafic magmatic activity, and stratigraphic evidence of recent regional uplift.

Collectively, these observations are consistent with dynamic support driven by mantle convection. However, the precise mechanism causing uplift remains enigmatic. Three possible endmembers include flow-driven uplift arising from upwelling plumes in the deep mantle, excess buoyancy due to warm mantle that has ponded within the asthenosphere, and quasi-isostatic uplift caused by thinning of the lithospheric mantle. Discriminating between these different mechanisms has been the focus of much debate within the geodynamics community (e.g. Moucha et al., 2008; Steinberger, 2016; Hoggard et al., 2017). In order to further investigate this issue, we examine two domes in detail— the Borborema Plateau of northeast Brazil and the Angolan dome of southwest Africa (Figure 1). These domes were chosen because they straddle the continent-ocean boundary at passive margins, which allows us to interrogate their structure and evolution using a diverse suite of continental and oceanic observations. Furthermore, both of these domes exhibit all of the characteristic features described above and boast a wealth of independent, but complementary, observational constraints.

In this study, we combine observations from river profile analysis, stratigraphic architecture and emergent marine terraces to place quantitative constraints on regional uplift histories. We estimate an upper bound for the temperature

Email address: marthe.kloecking@anu.edu.au (M. Klöcking)

and depth range of melting using the composition of mafic and ultramafic volcanic rocks. We infer present-day upper mantle temperatures from seismic tomographic models and reconstruct palaeogeothermal gradients using mantle xenoliths and xenocrysts from kimberlite pipes. By synthesising these independent constraints, we can investigate the relative importance of different mechanisms of topographic support.

2. Geological Setting

The Borborema Province of northeast Brazil is a Precambrian domain that lies on the Neoproterozoic mobile belt of the South American Platform, at the eastern end of the Brazilian shield (Almeida et al., 1981). It is bound to the west by the Parnaíba basin and to the south by the São Francisco craton. Most of this region is characterised by low relief, with relict mesas and plateaux at elevations of up to 1000 m (Figure 2). The most significant of these features is the Borborema Plateau, which has an elliptical shape with a northeast-southwest trending axis.

The southwest African passive margin comprises a series of Early to Mid-Cretaceous extensional sedimentary basins that developed during rifting of the Precambrian crystalline basement of the Congo craton (Ala and Selley, 1997). Its physiography is dominated by a long-wavelength, low relief planation surface with an elevation of 1 km, known as the *African surface*. This surface is punctuated by a series of 1000 km diameter swells that rise to $\sim$ 2.5 km and are centred on Angola, Namibia and South Africa (Figure 2; Sahagian, 1988; Burke and Gunnell, 2008). Here, we investigate the regional uplift of the most northerly of these domes that straddles the Angolan coastline between 9° and 16° south. The Angolan (or Bié) dome comprises portions of the Kwanza and Benguela Basins to the north and south, respectively. The highest elevations of this dome are found within the onshore Benguela Basin and reach altitudes of 2620 m.

The Borborema and Angolan domes both exhibit approximately radial drainage patterns. Offshore, anomalous oceanic residual depth measurements record present-day water-loaded support of up to +700 m near the Borborema dome and +1.2 km adjacent to the Angolan dome (Figure 2; Hoggard et al., 2017). Onshore, crustal thicknesses are 35–40 km (Laske et al., 2013). Seismic events are infrequent and of low magnitude, with less than five recorded earthquakes with $M_w > 5$ (CMT catalog; Dziewonski et al., 1981). Focal mechanism solutions and fault scarps record predominantly extensional or strike-slip motion. Tectonic activity appears to be restricted to a number of re-activated, deep lineaments that in northeast Brazil, trend from east-west through to north-south, and in Angola run northeast-southwest along a remnant extensional graben known as the Lucapa corridor (Almeida et al., 1981; Sykes, 1978). The lack of thrust faulting suggests that regional compression and associated crustal thickening do not play a role in maintaining domal topography. Estimates of elastic thickness obtained from either Bouguer coherence or free-air admittance analyses are $<$ 25 km for the Borborema Province, which indicates that long-wavelength topography is

not supported by flexure (Rodríguez Tribaldos et al., 2017). Unfortunately, ground-based gravity measurements used to constrain short-wavelength admittance values are unavailable for southwest Africa. Nevertheless, both domes have $\sim$ 40 mGal positive long-wavelength free-air gravity anomalies that coincide with low shear-wave velocity anomalies immediately beneath the lithospheric plate (75–125 km). These features suggest that dynamic support is at least partially responsible for present-day excess topography (Figure 2; Schaeffer and Lebedev, 2013; Bruinsma et al., 2014).

Neogene epeirogenic uplift has been described in both regions which overlaps in space and time with volcanic activity (Rodríguez Tribaldos et al., 2017; Roberts and White, 2010). In both cases, volcanism is concentrated in the vicinity of the peak amplitudes of free-air gravity anomalies, topographic swells, and of low shear wave velocity anomalies. Eruptions are more abundant in northeast Brazil, and extend over a longer time period (Giuliani et al., 2017; Guimarães et al., 2020). This activity has previously been attributed either to a plume located beneath Fernando de Noronha, to edge-driven convection, or to re-activation of lithospheric-scale fault zones (e.g. Rivalenti et al., 2000; Souza et al., 2005; Knesel et al., 2011). In Angola, a deep mantle upwelling has previously been invoked (Al-Hajri et al., 2009; Walker et al., 2016; Giuliani et al., 2017).

3. Epeirogenic Uplift

The two topographic domes considered here have been identified as having undergone 0.5–1.0 km of regional uplift within the last $\sim$ 30 Ma based upon a range of geological observations that include emergent marine terraces, perched deltaic deposits, regional erosional unconformities and palaeovalleys, and exhumation events observed in thermochronological studies (Bezerra et al., 2003; Jackson et al., 2005; Al-Hajri et al., 2009; Morais Neto et al., 2009; Guiraud et al., 2010; Colli et al., 2014; Walker et al., 2016; Rodríguez Tribaldos et al., 2017). In both locations, uplift significantly post-dates the most recent phase of active tectonic deformation, with rifting of the South Atlantic margins ceasing by Late Cretaceous times. Although widespread and well-resolved, these spot observations have limited spatial coverage. Drainage networks, on the other hand, are a ubiquitous feature of continental landscapes. The present-day geometry of a river profile is controlled by regional uplift and modulated by fluvial erosion, both of which can vary in space and time. With appropriate calibration of fluvial erosional processes, inverse modelling of suites of longitudinal river profiles can help to delineate spatio-temporal uplift histories (Roberts and White, 2010). Rivers on both the Borborema Plateau and the Angolan dome are characterised by radial drainage patterns with spatially consistent long-wavelength knickzones. Simultaneous inversion of these features yields calculated uplift histories that can be compared with the spot observations. Further details on the application of this methodology are given by Rodríguez Tribaldos et al. (2017).

3.1. Constraints for Borborema Province

Calibrated drainage analysis suggests that regional uplift of the Borborema Province occurred over the last ~ 30 Ma (Figure 3c; Rodríguez Tribaldos et al., 2017). Between 30 Ma and 10 Ma, uplift was steady at rates < 0.03 mm yr^{-1}, followed by a significant pulse within the last 10 Ma. A peak long-term rate of 0.06 ± 0.02 mm yr^{-1} is inferred.

Youthful emergence of the Borborema Province is corroborated by several independent observations (Rodríguez Tribaldos et al., 2017). The strongest evidence comprises relict Albian limestones of the Santana Formation which cap the Araripe Plateau in the centre of the Borborema Province at an elevation of 700–800 m (Figure 3a; Morais Neto et al., 2009). These rocks contain abundant marine fauna (Arai, 2014). Surrounding coastal margins are bounded by a series of emergent marine terraces of Pleistocene and Holocene age. These terraces occur at maximum elevations of ~ 80 m and ~ 4.5 m, respectively, and variations in their elevation along strike of the margin match the offshore patterns of oceanic residual depth measurements (Figure 3a; Bezerra et al., 2003; CPRM-Serviço Geológico do Brasil, 2004; Hoggard et al., 2017).

Inferred histories of uplift and denudation, especially for the last 20 Ma, also agree with exhumation events determined from thermochronological studies (Morais Neto et al., 2009). Apatite fission track analyses suggest that significant denudation occurred from 100–90 Ma and 20–0 Ma, with an additional minor event at 65–50 Ma. Miocene exhumation coincides with a transition from carbonate ramp to progradational clastic deposition in offshore sedimentary basins that surround both the northern and eastern margins, consistent with increased erosion rates onshore (Córdoba et al., 2007; Pessoa Neto et al., 2007). Figure 3c further illustrates that the timing of the most recent pulse of uplift coincides with a significant peak in onshore volcanic activity at 10 Ma.

3.2. Constraints for Angolan Dome

Evidence from shelf stratigraphy and drainage analysis suggests that the majority of uplift in Angola took place since Late Miocene times (post ~ 15 Ma), with an important earlier phase in Oligocene to Early Miocene times (35–20 Ma; Al-Hajri et al., 2009; Roberts and White, 2010). Continent-wide drainage analysis indicates that uplift rates peak at 0.07 mm yr^{-1} during Pliocene and Pleistocene times, and were more modest (~ 0.02 mm yr^{-1}) in the earlier phase (Figure 3f; O'Malley et al., under review). Any evidence for pre-Oligocene uplift events in Angola is obscured by the limited resolution of drainage analysis prior to Oligocene times.

As for the Borborema Province, there are multiple independent observations that corroborate these findings. Along the Kwanza and Benguela margins, a range of stratigraphic and geomorphological observations suggest that regional uplift predominantly occurred during Late Neogene and Quaternary times. Remnants of Cenomanian marine deposits are found along the rim of the Great Escarpment at elevations > 2000 m flanking the onshore Kwanza Basin

(Figure 3d; Sahagian, 1988). Within onshore portions of the basin, the stratigraphic succession shows that marine conditions prevailed until Early Pliocene times. Using planktonic biozonation, Jackson et al. (2005) identify five major depositional hiatuses that separate strata deposited in marine conditions. These hiatuses developed during Lower and Upper Oligocene, Early and Mid-Miocene and Plio-Pleistocene times (Figure 3f). The youngest marine sedimentary rocks, with abundant marine fossils, are found in the northern region of the onshore Kwanza Basin and are 5 Ma old. Much of the coastline is rimmed by sea cliffs and uplifted Pliocene marine terraces with maximum elevations of $\sim$ 100 m (Jackson et al., 2005). Within the southern part of the dome, the Benguela margin is characterised by a comparable stratigraphic succession with multiple hiatuses indicative of a similar history of moderate, punctuated uplift throughout the Cenozoic Era (Figure 3f; Guiraud et al., 2010). The distribution of Paleogene lateritic deposits, some of which drape parts of the dome, further suggests that relief was modest until Neogene times (Figure 3d; Burke and Gunnell, 2008).

Discontinuous Cenozoic deposition is also evident along the continental shelf. For example, erosional truncations of Lower Oligocene, Mid-Miocene and Plio-Pleistocene sediments occur within the Kwanza Basin (Jackson et al., 2005). The Mid-Miocene erosional unconformity coincides with an increase in terrigenous deposition and a switch from aggradational to progradational architecture (Lavier et al., 2001; Jackson et al., 2005; Al-Hajri et al., 2009). Although these unconformities are poorly studied, their proximity to erosionally bevelled shelves and coastal mountain ranges suggests that a significant component of offshore erosion is caused by uplift and tilting of the continental margin (Jackson et al., 2005). Moreover, denudation rates have been estimated from stacked seismic velocities by Al-Hajri et al. (2009), yielding post-Pliocene uplift rates of 0.4 mm yr^{-1} that coincide with the location of uplifted Pleistocene marine terraces along the coastal strip (Figure 3d; Hoggard et al., 2017). The timing of the youngest erosional surface is consistent with apatite fission track analyses from the onshore Kwanza Basin and from adjacent basement rocks that indicate onset of cooling events at $\sim$ 150 Ma, 150–100 Ma and 20–10 Ma (Jackson et al., 2005). Finally, as observed for the Borborema Province, peak uplift is synchronous with Pleistocene volcanic activity near the centre of the Angolan dome (Figure 3f).

4. Volcanic Activity

Epeirogenic uplift of Borborema and Angola has occurred in a series of punctuated phases that overlap in time with pulses of denudation and volcanic activity. These observations suggest that regional, sub-plate processes are at least partly responsible for the recent growth of these domes, which can be further assessed by investigating the geochemistry of the associated volcanic rocks.

In northeast Brazil, Cenozoic magmatism occurs across the Borborema Province, within the offshore Potiguar

Basin, and on the Fernando de Noronha archipelago (Sial et al., 1981; Knesel et al., 2011). It predominantly consists of alkaline plugs and necks, with compositions that range from basalt to trachybasalt, basanite and foidite. Lava flows are rare onshore, but abundant on Fernando de Noronha. Outcrops follow two geographical alignments, approximately north-south onshore and east-west offshore, that are thought to be controlled by the orientation of tectonic lineaments (Knesel et al., 2011). The north-south Macau-Queimadas Alignment runs through the state of Rio Grande do Norte into northern Paraíba. Here, outcrops consist predominantly of alkali basalts except within the Boa Vista and Potiguar Basins, both of which formed by Cretaceous rifting and contain the only known Cenozoic tholeiites in northeast Brazil (Sial et al., 1981; Souza et al., 2005). Magmatism occurs from 53–7 Ma with no obvious age progression ($^{40}Ar/^{39}Ar$ ages from Silveira, 2006, Knesel et al., 2011 and Guimarães et al., 2020). The Mecejana province, near the city of Fortaleza, is connected by an east-west trending chain of seamounts to the Fernando de Noronha archipelago. No samples have been recovered from these submarine outcrops, and so published studies necessarily focus on the two ends of this alignment. The rocks at Mecejana comprise a suite of phonotephritic plugs, domes, and dykes ranging between 35–30 Ma ($^{40}Ar/^{39}Ar$ ages from Guimarães et al., 2020). The island of Fernando de Noronha constitutes the tip of a 4 km high seamount that is built of a succession of alkaline lavas, plugs and pyroclastic deposits that have $^{40}Ar/^{39}Ar$ ages of 12.4–1.3 Ma (Perlingeiro et al., 2013).

In southwest Africa, kimberlites and carbonatites occur within the northeast-southwest oriented Lucapa corridor, a pre-existing extensional graben that is thought to have localised volcanic activity (Sykes, 1978; Giuliani et al., 2017). U-Pb ages from kimberlite pipes range from 238 Ma to 113 Ma (Eley et al., 2008; Robles-Cruz et al., 2012; Jelsma et al., 2013). In the Catanda region in the southern Kwanza Basin, a nephelinitic dyke has a K-Ar age of 92 ± 7 Ma (Torquato and Amaral, 1973). Further north in the Kwanza Basin, tholeiites yield $^{40}Ar/^{39}Ar$ ages of $\sim$ 132 Ma while an alkaline lava flow is dated at 95 ± 2 Ma (Marzoli et al., 1999). The only known post-Cretaceous activity in Angola comprises Pleistocene carbonatites and aillikites of the Catanda volcanic complex within the Lucapa corridor ($^{40}Ar/^{39}Ar$ ages of $\sim$ 500–800 ka; Giuliani et al., 2017). The Pleistocene Catanda volcanic exposures lie within a local graben delimited by three intersecting sets of faults that feed active geothermal systems (Campeny et al., 2014). Outcrop occurs on sediment-covered, eroded hills and is dominated by pyroclastic beds, with minor lava flows that reach maximum thicknesses of 50 m.

4.1. Geochemical Characteristics

51 samples were collected on Fernando de Noronha during August and September 2014. 32 samples were collected from the Borborema Province in October 2015. These rocks were analysed for major and selected trace elements using X-ray fluorescence (XRF) spectrometry at the University of Edinburgh, and for trace and rare earth elements using inductively coupled plasma mass spectrometry (ICP-MS) at the University of Cambridge. Analyses

were screened for concentrations of SiO_2 > 40 wt% and MgO > 7 wt%. This dataset was supplemented by published analyses from Fodor et al. (1998), Lopes (2002), Rivalenti et al. (2007), Lopes and Ulbrich (2015) and Ngonge et al. (2016). The final inventory contains 56 samples from the Borborema Province and 34 from Fernando de Noronha. 10 analyses from the Angolan dome that contain MgO > 8 wt% were selected from Campeny et al. (2015). Complete data tables are provided in Supplementary Materials, together with further details concerning sample screening and analytical procedures.

There is minimal evidence for contamination by continental crustal material in the Brazilian samples, based upon both Ce/Pb and La/Nb trace element ratios and Sr-Nd-Pb isotopic compositions (Sial et al., 1981; Ngonge et al., 2016). Instead, there is overlap with the compositional range of ocean island basalts. The aillikites from the Angolan dome are clearly distinct from the largely alkaline basalts of northeast Brazil. In particular, they have low SiO_2, high concentrations of CaO and volatiles, and a much greater enrichment of all trace elements except Cs, Rb, Pb and Hf, which are characteristic features of these hydrous, carbonated melts (Campeny et al., 2015). Their isotopic compositions are also very similar to ocean island basalts, indicating that Catanda melts may have an origin in the mantle with minimal contamination from continental crust. However, unlike the Brazilian examples, they exhibit lead isotopic signatures characteristic of the HIMU mantle array widely observed in African volcanic provinces (Campeny et al., 2015; Giuliani et al., 2017).

4.2. Magmatic Source Conditions

We select the most primitive melts from each of the three provinces to estimate the depth range and potential temperature of melting using the near-fractional decompression melting model developed by McKenzie and O'Nions (1991). Assuming a source composition and elemental partition coefficients, observed rare earth element (REE) concentrations are fitted by varying melt fraction as a function of depth in an inverse scheme. The composition of other elements is subsequently predicted by forward modelling, providing an independent means to assess the quality of our results. This approach exploits the partitioning behaviour of trace elements, which renders REE distributions sensitive to cumulative melt fraction and to the relative proportions of melting that occur within the garnet and spinel stability fields. We define the spinel-garnet transition zone at 63–72 km (i.e. 21–24 kbar). This range is derived from the results of thermodynamic modelling by Jennings and Holland (2015) and has been extended to slightly greater depths to ensure that the transition is fully resolved by the melting model. Potential temperature is estimated by comparison of the optimal melt fraction distribution to suites of decompression melting paths (Katz et al., 2003). The ambient mantle potential temperature of this parameterisation is ~1330 °C, which is required to produce 7 km of basaltic crust at a mid-ocean spreading ridge. We propose that the top of the melting column constitutes the base of the mechanical lithosphere, beyond which further upwelling of asthenospheric material is inhibited.

Our primary goal is to investigate the possible presence of anomalously hot asthenospheric material beneath the plate that could be responsible for uplift of the Borborema and Angolan domes. We therefore aim to use melt geochemistry to place upper bounds on mantle potential temperature, as well as infer the depth range from which melts are sourced. For the source composition, we assume a dry, primitive peridotite mantle. Whilst metasomatic contributions have been invoked in the formation of alkali basalts and aillikites, the addition of water or CO_2 will act to significantly lower the solidus and reduce the inferred potential temperature (e.g. Katz et al., 2003; Foley et al., 2009). Thus a satisfactory fit to REE compositions achieved from our dry peridotite source will represent an end-member case and an upper bound on mantle temperature.

Typical uncertainties associated with this modelling approach are ±3 % in cumulative melt fraction and ±10 km in the top of the melting column, which results in variations of ±30 °C in inferred potential temperature (Brodie et al., 1994; Klöcking et al., 2018). The use of an alternative melting parameterisation or a deeper spinel-garnet transition, for example due to higher concentrations of Cr or Fe^{3+} in the source, tends to increase inferred potential temperature by up to +50°C (Klöcking et al., 2018).

4.3. Constraints for northeast Brazil

Volcanic compositions from the Borborema Province are best fit with 2.5 % melting of a dry, primitive mantle source (Figure 4a–4c). Root-mean-squared (RMS) misfit between observed and calculated REE concentrations is < 0.5. Melts are generated between 61–73 km depth, entirely within the spinel stability field and for the most part within the spinel-garnet transition zone. High average MgO concentrations of these samples indicate that very small amounts of olivine fractionation ($\sim$ 7%) occurred prior to eruption. The calculated melt fraction distribution with depth is consistent with ambient potential temperature in the range of 1330–1340°C. Forward-modelled fits to remaining trace and major elements are also acceptable, except for small residual misfits for Rb, K, Pb, Ta, Nb and Sr. It is likely that these discrepancies indicate either post-emplacement surface alteration or minor contributions from metasomatic lithospheric melts.

REE compositions from Fernando de Noronha can be reproduced with 1% melting over a depth range of 63–73 km (Figure 4d–4f). Major element compositions indicate $\sim$ 22% fractionation of olivine. Melting occurs entirely within the spinel-garnet transition zone and is consistent with ambient mantle potential temperature (i.e. $\sim$ 1320°C). Model fit to REE concentrations is satisfactory, but less good than for Borborema samples (RMS misfit < 1.2). There are minor discrepancies in Ta, Nb and Sr concentrations. Remaining trace and major elements are accurately matched with the exception of large ion lithophile elements (LILEs), whose predicted values are significantly higher than observed (Figure 4e).

Discrepancies between observed and calculated concentrations of highly incompatible elements for Fernando de Noronha may be the result of sea-water alteration, as evidenced by significant Na depletion (Guimarães et al., 2020). An additional factor is that these alkaline rocks have low melt fractions, which raises three potential issues. First, there is a paucity of experimental constraints on element partitioning at small melt fractions, yielding less reliable results for melt modelling (McKenzie and O'Nions, 1991). Second, for small melt fractions, the final melt composition is more sensitive to contributions from highly enriched lithospheric melts. Third, although we observe no unusual crystal phases in thin section, incipient fractionation of minerals such as melilite could have modified the trace element composition of these silica-undersaturated magmas. Thus, Fernando de Noronha magmas may be affected by enrichment through metasomatic melts from the base of the lithosphere. A more enriched source composition would require a larger melt fraction to dilute REE concentrations sufficiently to match the observations. Larger melt volumes and a higher volatile content would facilitate extraction of these magmas. However, the result that no excess mantle temperature is predicted for this region is robust to this additional metasomatic melting process.

Both Borborema Province and Fernando de Noronha can be satisfactorily modelled using the same primitive mantle source composition. Although asthenospheric melting was assumed in both cases, we find evidence for minor additional contributions from metasomatised lithosphere. This inference is consistent with other petrographic and isotopic studies. For example, Fodor et al. (2002) argue that enrichment of Fe and Ti in porphyroclastic xenoliths and light REEs in protogranular xenoliths is an indicator of metasomatism. It has also been suggested that the textures and Nd-Sr isotopic signatures of mantle xenoliths from Fernando de Noronha are indicative of deformation and thermochemical modification associated with infiltration of asthenospheric alkali melts into the base of the lithosphere (Rivalenti et al., 2000, 2007). No mantle potential temperature anomaly is required to generate these Brazilian melts, although up to + $\sim$ 25°C would be permissible.

4.4. Constraints for Angola

It is not possible to fit REE concentrations of the Catanda aillikites using a single-stage melting event for a dry, primitive peridotite mantle source. Instead, a significant contribution from a metasomatised (i.e. hydrated and/or carbonated) lithospheric mantle is required. We separately generate an asthenospheric and a metasomatic melt, before mixing them together to obtain a final melt composition (Figures 4g–4i). This process is analogous to upwards transport of a small volume of hot asthenospheric melt that subsequently triggers remobilisation of metasomatic material previously frozen into the lithosphere. Given the high content of incompatible elements in the metasomatic source, the trace element composition of the final aillikite will be dominated by that of the metasomatic melt.

The composition of metasomatised mantle lithosphere is poorly known. Here, we have chosen to follow the procedure proposed for kimberlite melting by Tainton and McKenzie (1994) with several significant modifications.

First, we simulate the generation of cratonic lithosphere by melting a primitive mantle source by 21.5 % over a depth range of 0–90 km to produce a highly depleted residuum. Second, to simulate metasomatic refertilisation, this residue is subsequently enriched 8 % by volume with a small-fraction melt ($\sim$ 0.5%), generated from primitive mantle in the garnet stability field. This metasomatised cratonic material is then used as a source composition to generate the metasomatic component of modern Catanda aillikite melts. To approximate melting of a hydrous and carbonated metasomatic vein, we have included amphibole as a major mineral phase in this source and use the carbonatite partition coefficients of Dasgupta et al. (2009).

For the asthenospheric melt that triggers melting of metasomatic material, primitive mantle is melted $\sim$ 0.2% in the garnet stability field at a potential temperature of $\sim$ 1380°C. Optimal fits to observed REE concentrations are obtained with a maximum metasomatic melt fraction of 1.2 %, which must be generated within the spinel stability field (Figure 4i). There is a trade-off between the melt fraction of the asthenospheric contribution and that of the metasomatic melt. Large residual misfit values for LILEs, Ta, Zr and Hf are evidence of the considerable uncertainty surrounding both the asthenospheric and the metasomatic source compositions, their mineralogy, and the appropriate partition coefficients (Figure 4h). Our relatively simple approach may therefore not capture the full complexities of aillikite genesis. For example, a HIMU source has been invoked for Catanda aillikites, which is thought to be derived from recycled crustal material in the convecting mantle (Giuliani et al., 2017). The precise composition of this mantle reservoir remains controversial, however, and it is therefore challenging to model. We suggest that our ability to match aillikite REE compositions using primitive mantle with a metasomatic contribution yields an important upper bound on melt generation beneath Angola, since the increased fertility of HIMU would reduce estimated mantle potential temperature. Thus, geochemical compositions permit a maximum sub-plate thermal anomaly of ~50 °C. We discuss other options for metasomatic composition, mineralogy, and aillikite genesis in the Supplementary Material.

5. Present-day Thermal Structure of the Upper Mantle

To investigate possible mechanisms for regional uplift, it is useful to determine the present-day buoyancy structure of the lithospheric and asthenospheric mantle. Inverse modelling of geochemical measurements yields spot estimates of sub-plate temperature and the depth-extent of the melting region. Seismic tomographic models provide a complementary perspective, but they require careful calibration in order to convert seismic velocity into temperature. Here, we start with the SL2013sv global shear wave model of Schaeffer and Lebedev (2013). This model is augmented by the SA2019 regional model of Celli et al. (2020), which is constructed from over 1.2 million seismograms and provides unprecedented ray path coverage beneath Africa and South America. It uses a combination of body and surface waves over periods of 10–450 s, which are sensitive to the shear-wave velocity structure of the upper $\sim$ 300 km

of the mantle. The model has a horizontal knot spacing of ~ 325 km and nominal vertical resolution of 25–50 km. These particular models have been selected because they yield good correlations with independent databases such as the geoid, observed dynamic topography, mid-ocean ridge geochemistry, sediment-hosted base metal deposits, and thermobarometry on mantle xenoliths and xenocrysts (Steinberger, 2016; Hoggard et al., 2017; Davies et al., 2019; Hoggard et al., 2020; Richards et al., under review).

In northeast Brazil, thick lithosphere of the São Francisco craton to the south of the Borborema Province and of the Brazilian shield to the west are manifest by fast velocity anomalies down to a depth of 200 km (Figure 5). Slow velocity anomalies lie north and northeast of the continent and extend out to Fernando de Noronha. At depths shallower than ~ 200 km, these low velocities also extend beneath the eastern edge of the Borborema Province, coinciding with the distribution of Cenozoic volcanism. In southwest Africa, fast velocities of the Congo craton extend down to at least 200 km and there is a marked slow velocity region beneath the Angolan dome itself. This anomaly continues to greater depth than the Brazilian equivalent and appears to form a roughly east-west trending corridor that extends out beneath the oceanic plate.

Here, we convert seismic velocities to temperature using the approach of Richards et al. (under review), which builds on a methodology originally described by Priestley and McKenzie (2006). We adopt a parameterisation for anelasticity at seismic frequencies from Yamauchi and Takei (2016) which is calibrated using independent constraints that include the thermal structure of oceanic lithosphere, adiabatic temperatures of the deeper mantle, seismic attenuation measurements, and the bulk viscosity of upper mantle obtained from studies of glacial isostatic adjustment. In contrast to previous studies, we do not include pressure-temperature constraints derived from thermobarometric analysis of mantle xenoliths.

Profiles of seismic velocity and inferred temperature as a function of depth have been extracted for the Borborema Province, for Fernando de Noronha, and for the Catanda region in Angola (Figure 5). To account for the limited horizontal resolution of seismic tomographic models, an area with a 1° radius was sampled and averaged in each case. The Borborema profile has the fastest velocities, and therefore the coldest inferred temperatures, while results from Fernando de Noronha and Angola are comparable within uncertainty. Temperatures are close to the 1330 °C adiabat, but could be as high as 1380 °C. Calculated temperature profiles do not cross the dry peridotite solidus. Instead, the presence of at least 0.1 wt% water or CO_2 in the mantle source might be required in order to generate magmatism (Katz et al., 2003; Foley et al., 2009). This inference is consistent with the calibrated anelastic parameters, which include a solidus gradient of ~ 1°C km^{-1} that matches either wet or CO_2-rich solidus parameterisations. Thus there is no direct evidence for significant sub-plate thermal anomalies greater than ~ 50°C beneath these topographic domes.

6. Cretaceous Thermal Structure of the Lithosphere

To investigate possible contributions to Neogene uplift from thinning of the lithosphere, we require constraints on its past thermal structure. These constraints can be obtained from thermobarometric studies of mantle material (xenoliths or xenocrysts) that is entrained and carried to the surface in volcanic rocks. Most shallow mantle rocks are aluminous lherzolites which contain olivine, chrome-rich clinopyroxene, and orthopyroxene, with additional minor phases of spinel or garnet depending on equilibration depth. Laboratory experiments have shown that pressure- and temperature-dependent chemical exchange occurs between these different phases, so that compositions of each mineral can be used to infer the depth and temperature of xenolith equilibration. The most reliable thermobarometers are available for garnet-bearing assemblages and have been extensively calibrated against laboratory samples (Nimis and Grütter, 2010). Cenozoic volcanic rocks from central Borborema contain only spinel lherzolites, consistent with a base of the lithosphere that is shallower than the spinel-garnet transition. Their youth prevents us from constraining its thermal structure at earlier times (e.g. Rivalenti et al., 2000; Fodor et al., 2002; Liu et al., 2019). However, southwest Africa contains numerous Cretaceous kimberlites that carry garnet-bearing material that is suitable for thermobarometric analysis.

We have compiled xenolith and xenocryst compositions from three different regions (Figure 6b; Supplementary Material; Boyd and Danchin, 1980; Pivin et al., 2009; Robles-Cruz et al., 2012). The first is located at the centre of the Angolan dome and consists of the Somacuanza (dated to 134 Ma) and Artur de Paiva (undated) kimberlites. The second region lies along the northeast margin of the dome and contains four kimberlites: Alto Cuilo-63 (129 Ma), Tchiuzo (121 Ma), Catoca (118 Ma), and Camutue (undated). The third location is the Mbuji-Mayi kimberlite in the south of the central Democratic Republic of Congo, dated to 70 Ma. Since the majority of available compositions of entrained material are from heavy mineral concentrates obtained by diamond exploration, knowledge of which mineral phases come from the same xenolith has been lost. We therefore adopt the Nimis and Taylor (2000) thermobarometer that requires only the oxide composition of individual chrome-diopside grains to be known. The barometer exploits the exchange of chromium between clinopyroxene and garnet, whilst the thermometer uses enstatite-in-diopside, requiring that both garnet and orthopyroxene were also present in the xenolith source. The thermometer and barometer equations are inter-dependent and are solved by iteration to determine optimal pressure-temperature (P-T) xenocryst equilibration conditions. Pressure is converted into depth assuming a lithostatic pressure gradient of $\frac{1}{30}$ GPa km^{-1}. We only use diopside compositions that pass the two cation and oxide checks suggested by Nimis and Grütter (2010), and discard values with either T < 700 °C or depths shallower than 60 km, where this thermobarometer is believed to become inaccurate. Laboratory calibrations yield one standard deviation uncertainties of ±30°C and ±7 km (Nimis and Grütter, 2010). Errors associated with oxide measurement uncertainty from microprobe analysis introduce a covarying

uncertainty of approximately ±50°C and ±5 km (Mather et al., 2011). Both uncertainties are small compared to the typical P-T spread for the ensemble of individual clinopyroxenes.

P-T estimates form generally linear arrays of increasing temperature with depth, covering a depth range of 90–140 km in central Angola, 80–190 km in northeast Angola, and 150–225 km in southern Congo (Figures 6c–6e). For each locality, these data are entered into the FITPLOT algorithm to determine the best-fitting palaeogeothermal gradient (Mather et al., 2011). We assume a 40 km-thick crustal layer with constant conductivity of 2.5 W m^{-1} $°C^{-1}$ and radiogenic heat production of 1.12 μW m^{-3} and 0.40 μW m^{-3} in the upper and lower halves, respectively. Mantle potential temperature is fixed at 1333 °C and olivine conductivity in the mantle is assumed to vary as a function of pressure and temperature.

Two important observations emerge from this analysis that have ramifications for the geodynamic evolution of the Angolan dome. First, a spatial gradient in lithospheric thickness was already present during Cretaceous times. The transition from conductive to adiabatic temperature gradient deepens from ~ 160 km in central Angola to ~ 220 km in the northeast and down to ~ 270 km in southern Congo. Second, the present-day geothermal gradient obtained from the SA2019 tomographic model matches the Cretaceous gradients in Congo and northeast Angola, but it is significantly hotter beneath the Angolan dome where the lithosphere has thinned by ~ 30 km.

7. Mechanisms of Dynamic Uplift

Based on these multiple strands of evidence which are summarised in Figure 7, we evaluate three possible mechanisms that may be responsible for the observed domal uplift: flow-driven uplift above a major mantle upwelling; thermal isostatic uplift generated by a warm asthenospheric layer; and isostatic uplift caused by lithospheric thinning.

There is limited evidence to favour flow-driven uplift above major mantle upwellings in the two examples examined here. Most seismological studies are unable to image low velocity vertical conduits that could be related to a plume in either location, although a large low velocity anomaly occurs in the deep mantle beneath Africa and is likely to be responsible for long-wavelength topographic support across the sub-equatorial continent (Lithgow-Bertelloni and Silver, 1998; Gurnis et al., 2000). Using P-wave receiver functions, Pinheiro and Julià (2014) find that there is no evidence for thinning of the mantle transition zone beneath the Borborema Province. They argue that any thermal perturbation is limited to the upper mantle. Although hot spot tracks have been suggested for both onshore and offshore Brazilian magmatism, no obvious age-progression is observed (e.g. Guimarães et al., 2020). The orthogonal orientation to plate motion and to other known hotspot tracks, as well as a mismatch between observed and required plate velocity, further weaken this hypothesis. In Angola, seismological evidence for the presence or absence of a deep upwelling plume is limited. Although a relatively continuous low shear-wave velocity finger running at

an angle from Angola down to the African Large Low Shear Velocity Province has been interpreted based on one seismic tomography model (Giuliani et al., 2017), it is absent in other models. Furthermore, the paucity and small volume of volcanic activity, combined with its low inferred potential temperatures, suggest that there is unlikely to be a significant upwelling mantle plume underlying the dome.

The role of warm asthenospheric material can be explored using a simple model. By including the effect of thermal expansivity, the magnitude of air-loaded isostatic uplift, U_a, caused by the introduction of hot material in a sub-plate layer or channel depends upon its thickness and excess temperature according to

$$U_a = \frac{h\alpha\Delta T}{1 - \alpha T_\circ} \tag{1}$$

where h is layer thickness, $\alpha = 3 \times 10^{-5}$ °C^{-1} is thermal expansivity of mantle material, and ΔT is its excess temperature above the background value $T_\circ = 1330$°C. This mechanism has been previously invoked for both the Borborema and Angolan domes. Brazilian magmatism has been linked to channelling of hotspot material along a lithospheric fracture zone (Sykes, 1978). Simões Neto et al. (2018) use P-wave tomography to invoke a low-velocity zone at depths of 100–400 km that coincides with the surface expression of the Borborema Province, which they attribute to lateral flow of low-velocity material from a mantle plume located to the southwest. In both regions, elevated surface heat flow of $\sim$ 70–80 mW m^{-2} is observed which, combined with positive long-wavelength free-air gravity anomalies and slow sub-plate shear wave velocities, is also consistent with excess asthenospheric temperatures (Fodor et al., 2002; Lucazeau, 2019). Here, we have found no evidence for an asthenospheric thermal anomaly that is significantly greater than $\sim$ 50°C, based on either shear wave velocities or volcanic geochemistry. Adopting a layer thickness of $h = 150 \pm 50$ km from surface wave images, Equation (1) suggests that emplacement of this hot material can account for no more than 235 ± 80 m of uplift, which is smaller than the 0.5–1.0 km determined by truncated shelf stratigraphy and drainage analysis (Al-Hajri et al., 2009; Roberts and White, 2010; Rodríguez Tribaldos et al., 2017).

Finally, we investigate the role of lithospheric thinning. The magnitude of air-loaded isostatic uplift, U_l, generated by lithospheric thinning can be calculated from

$$U_l = \frac{\alpha T_\circ}{2(1 - \alpha T_\circ)} \left[\Delta z + \frac{z_c(z_l - z_c - \Delta z)}{z_l - \Delta z} - \frac{z_c(z_l - z_c)}{z_l} \right] \tag{2}$$

where z_l is the original lithospheric thickness, Δz is the amount of lithospheric mantle thinning, and z_c is crustal thickness. In Angola, the comparison between Cretaceous geothermal gradients from xenocryst thermobarometry with the present-day gradients from the SA2019 tomographic model suggests that the lithosphere beneath the centre of the dome was originally $\sim$ 150 km thick and may have been thinned by $\sim$ 30 ± 10 km since 120 Ma. Given a

crustal thickness of ~ 40 km, Equation (2) shows that this thinning yields 0.6 ± 0.2 km of air-loaded uplift, which is a significant contribution to the observed vertical motion. In comparison, lithosphere beneath northeast Angola and southern Congo appears to be largely unmodified during this period. Our uplift estimate represents an upper bound since chemical depletion of the original lithospheric mantle will act to reduce this value, which would produce zero net uplift if lithospheric depletion reaches 60 kg m^{-3}.

It is not possible to carry out a similar calculation for the Borborema Province since no reliable thermobarometer yet exists for spinel lherzolites. The likely difference in lithospheric thickness between the two domes is probably the most significant reason for differences in volume and composition of mafic magmatism. In both locations, only very small melt fractions are generated beneath the plate, so that the surface distribution of volcanism is probably determined by pre-existing lithospheric weaknesses. Inverse modelling of volcanic compositions suggests that the lithospheric thickness of northeast Brazil is ~ 60 km, consistent both with seismological constraints and with the lack of garnet in mantle xenoliths. Nonetheless, geothermometers have been applied to xenolith suites and, in combination with microstructural arguments relating to annealing textures in the samples, suggest that young (between Cretaceous and recent) deformation and modification of the deeper lithosphere has occurred (Liu et al., 2019). Hence lithospheric thinning is probably also a significant factor beneath northeast Brazil.

In summary, the topographic domes of northeast Brazil and southwest Africa are generated and maintained by modest asthenospheric thermal anomalies that have thinned the overlying lithosphere. An original lithospheric gradient across southwest Africa existed in Cretaceous times which may be associated with continental break-up or earlier extensional events. Subsequently, this basal topography may have been responsible for channelling asthenospheric flow towards the dome, as invoked by Giuliani et al. (2017), which in turn has triggered additional lithospheric thinning. The exact nature of this thinning is unclear. Purely thermal erosion by conductive heating from below is unlikely to have been significant, since the thermal anomaly is small and time scales of thermal diffusion are large. Mechanical erosion by repeated melt infiltration into the base of the lithosphere can, in contrast, trigger thinning at rates of several kilometres per million years (Havlin et al., 2013). An alternative explanation is that these lateral temperature gradients in the shallow mantle led to the onset of small-scale, edge-driven convection that further mechanically eroded the lithosphere. Indeed, such an upper mantle flow regime has previously been suggested for the Borborema Province (e.g. Knesel et al., 2011; Pinheiro and Julià, 2014).

8. Conclusions

To investigate the origin of intraplate topographic domes, we have analysed two examples from northeast Brazil and southwest Africa. We combine quantitative constraints from drainage profiles, stratigraphic architecture, emer-

gent marine terraces, volcanic geochemistry, thermobarometry of mantle xenocrysts, and upper mantle shear wave velocities. The majority of topographic growth of both the Borborema and Angolan domes occurred within the last 30 Ma, which significantly post-dates known tectonic activity. Regional uplift appears to be episodic and overlaps with volcanic activity and denudation estimates. Neither volcanic trace element chemistry nor seismic velocities in the upper mantle support the existence of large-scale thermal anomalies. However, the present-day lithosphere is thin: less than 100 km beneath Angola and as little as 60 km beneath Borborema. Furthermore, geothermal gradients calculated from mantle xenocrysts demonstrate a $\sim$ 30 km thinning of the lithosphere beneath central Angola some time between 120 Ma and the present-day. We conclude that the most plausible mechanism for regional uplift is emplacement of warm asthenosphere beneath the plate, combined with significant lithospheric thinning caused by thermomechanical erosion.

9. Acknowledgements

This research project was funded by BP as part of the Parnaíba Basin Analysis Project. MH acknowledges support from the Donors of American Chemical Society Petroleum Research Fund (59062-DNI8). P. Ball and B. Carvalho assisted with field work in Brazil. We are also grateful to R. Clarke, R. Davies, J. Day, J.G. Fitton, N. Odling, C. O'Malley, S. Stephenson, and M. Walker for their help. We thank H.-P. Bunge and A. Giuliani for insightful reviews. Figures were prepared using Generic Mapping Tools software. Geochemical analyses are given in online Supplementary Material and references therein. New samples will be registered with IGSNs in SESAR (www.geosamples.org) and included within the EarthChem portal (www.earthchem.org). University of Cambridge contribution number esc.XXXX.

References

Al-Hajri, Y., White, N., Fishwick, S., 2009. Scales of transient convective support beneath Africa. Geology 37, 883–886.

Ala, M., Selley, R., 1997. The west African coastal basins, in: Sedimentary Basins of the World. Elsevier. volume 3, pp. 173–186.

Almeida, F., Hasui, Y., Brito Neves, B., Fuck, R., 1981. Brazilian structural provinces: An introduction. Earth-Science Reviews 17, 1–29.

Arai, M., 2014. Aptian/Albian (Early Cretaceous) paleogeography of the South Atlantic: A paleontological perspective. Brazilian Journal of Geology 44, 339–350.

Bezerra, F.H.R., Barreto, A.M., Suguio, K., 2003. Holocene sea-level history on the Rio Grande do Norte state coast, Brazil. Marine Geology 196, 73–89.

Boyd, F., Danchin, R., 1980. Lherzolites, eclogites and megacrysts from some kimberlites of Angola. American Journal of Science 280-A, 528–549.

Brodie, J., Latin, D., White, N., 1994. Rare earth element inversion for melt distribution: Sensivity and application. Journal of Petrology 35, 1155–1174.

Bruinsma, S.L., Förste, C., Abrikosov, O., Lemoine, J.M., Marty, J.C., Mulet, S., Rio, M.H., Bonvalot, S., 2014. ESA's satellite-only gravity field model via the direct approach based on all GOCE data. Geophysical Research Letters 41, 7508–7514.

Burke, K., Gunnell, Y., 2008. The African erosion surface: A continental-scale synthesis of geomorphology, tectonics, and environmental change over the past 180 million years. Geological Society of America Memoirs 201, 1–66.

Campeny, M., Kamenetsky, V.S., Melgarejo, J.C., Mangas, J., Manuel, J., Alfonso, P., Kamenetsky, M.B., Bambi, A.C., Gonçalves, A.O., 2015. Carbonatitic lavas in Catanda (Kwanza Sul, Angola): Mineralogical and geochemical constraints on the parental melt. Lithos 232, 1–11.

Campeny, M., Mangas, J., Melgarejo, J.C., Bambi, A., Alfonso, P., Gernon, T., Manuel, J., 2014. The Catanda extrusive carbonatites (Kwanza Sul, Angola): An example of explosive carbonatitic volcanism. Bulletin of Volcanology 76, 1–15.

Celli, N.L., Lebedev, S., Schaeffer, A.J., Ravenna, M., Gaina, C., 2020. The upper mantle beneath the South Atlantic Ocean, South America and Africa from waveform tomography with massive data sets. Geophysical Journal International 221, 178–204.

Colli, L., Stotz, I., Bunge, H.P., Smethurst, M., Clark, S., Iaffaldano, G., Tassara, A., Guillocheau, F., Bianchi, M.C., 2014. Rapid South Atlantic spreading changes and coeval vertical motion in surrounding continents: Evidence for temporal changes of pressure-driven upper mantle flow. Tectonics 33, 1304–1321.

Córdoba, V.C., Jardim de Sá, E.F., do Carmo Sousa, D., Antunes, A.F., 2007. Bacia de Pernambuco-Paraíba. Boletim de Geociencias da Petrobras 15, 391–403.

CPRM-Serviço Geológico do Brasil, 2004. Carta Geológica do Brasil ao Milionésimo: Sistema de informações geográficas-SIG [Geological Map of Brazil 1:1.000.000 scale: Geographic information system-GIS].

Dasgupta, R., Hirschmann, M.M., McDonough, W.F., Spiegelman, M., Withers, A.C., 2009. Trace element partitioning between garnet lherzolite and carbonatite at 6.6 and 8.6 GPa with applications to the geochemistry of the mantle and of mantle-derived melts. Chemical Geology 262, 57–77.

Davies, D.R., Valentine, A.P., Kramer, S.C., Rawlinson, N., Hoggard, M.J., Eakin, C.M., Wilson, C.R., 2019. Earth's multi-scale topographic response to global mantle flow. Nature Geoscience 12, 845–850.

Dziewonski, A.M., Chou, T.A., Woodhouse, J.H., 1981. Determination of earthquake source parameters from waveform data for studies of global and regional seismicity. Journal of Geophysical Research 86, 2825–2852.

Eley, R., Grütter, H., Louw, A., Tunguno, C., Twidale, J., 2008. Exploration geology of the Luxinga kimberlite cluster (Angola) with evidence supporting the presence of kimberlite lava, in: International Kimberlite Conference, Extended Abstracts, University of Alberta.

Fodor, R.V., Mukasa, S.B., Sial, A.N., 1998. Isotopic and trace-element indications of lithospheric and asthenospheric components in Tertiary alkalic basalts, northeastern Brazil. Lithos 43, 197–217.

Fodor, R.V., Sial, A.N., Gandhok, G., 2002. Petrology of spinel peridotite xenoliths from northeastern Brazil: Lithosphere with a high geothermal gradient imparted by Fernando de Noronha plume. Journal of South American Earth Sciences 15, 199–214.

Foley, S., Yaxley, G., Rosenthal, A., Buhre, S., Kiseeva, E., Rapp, R., Jacob, D., 2009. The composition of near-solidus melts of peridotite in the presence of CO2 and H2O between 40 and 60 kbar. Lithos 112, 274 – 283.

Giuliani, A., Campeny, M., Kamenetsky, V.S., Afonso, J.C., Maas, R., Melgarejo, J.C., Kohn, B.P., Matchan, E.L., Mangas, J., Gonçalves, A.O., Manuel, J., 2017. Southwestern Africa on the burner: Pleistocene carbonatite volcanism linked to deep mantle upwelling in Angola. Geology 45, 971–974.

Guimarães, A.R., Fitton, J.G., Kirstein, L.A., Barfod, D.N., 2020. Contemporaneous intraplate magmatism on conjugate South Atlantic margins: A hotspot conundrum. Earth and Planetary Science Letters 536, 116–147.

Guiraud, M., Buta-Neto, A., Quesne, D., 2010. Segmentation and differential post-rift uplift at the Angola margin as recorded by the transform-rifted Benguela and oblique-to-orthogonal-rifted Kwanza basins. Marine and Petroleum Geology 27, 1040–1068.

Gurnis, M., Mitrovica, J.X., Ritsema, J., van Heijst, H.J., 2000. Constraining mantle density structure using geological evidence of surface uplift rates: The case of the African Superplume. Geochemistry, Geophysics, Geosystems 1.

Havlin, C., Parmentier, E.M., Hirth, G., 2013. Dike propagation driven by melt accumulation at the lithosphere-asthenosphere boundary. Earth and Planetary Science Letters 376, 20–28.

Hoggard, M.J., Czarnota, K., Richards, F.D., Huston, D.L., Jaques, A.L., Ghelichkhan, S., 2020. Global distribution of sediment-hosted metals controlled by craton edge stability. Nature Geoscience .

Hoggard, M.J., White, N., Al-Attar, D., 2016. Global dynamic topography observations reveal limited influence of large-scale mantle flow. Nature Geoscience 9, 456–463.

Hoggard, M.J., Winterbourne, J., Czarnota, K., White, N., 2017. Oceanic residual depth measurements, the plate cooling model, and global dynamic topography. Journal of Geophysical Research: Solid Earth 122, 2328–2372.

Jackson, M.P., Hudec, M.R., Hegarty, K.A., 2005. The great West African Tertiary coastal uplift: Fact or fiction? A perspective from the Angolan divergent margin. Tectonics 24.

Jelsma, H., Krishnan, U., Perritt, S., Preston, R., Winter, F., Lemotlo, L., van der Linde, G., Armstrong, R., Phillips, D., Joy, S., Costa, J., Facatino, M., Posser, A., Kumar, M., Wallace, C., Chinn, I., Henning, A., 2013. Kimberlites from central Angola: A case study of exploration findings, in: Pearson, D.G., Grütter, H.S., Harris, J.W., Kjarsgaard, B.A., O'Brien, H., Rao, N.V.C., Sparks, S. (Eds.), Proceedings of 10th International Kimberlite Conference. Springer India, New Delhi, pp. 173–190.

Jennings, E.S., Holland, T.J., 2015. A simple thermodynamic model for melting of peridotite in the system NCFMASOCr. Journal of Petrology 56, 869–892.

Katz, R.F., Spiegelman, M., Langmuir, C.H., 2003. A new parameterization of hydrous mantle melting. Geochemistry, Geophysics, Geosystems 4, 1–19.

Klöcking, M., White, N.J., Maclennan, J., McKenzie, D., Fitton, J.G., 2018. Quantitative relationships between basalt geochemistry, shear wave velocity, and asthenospheric temperature beneath western North America. Geochemistry, Geophysics, Geosystems 19, 3376–3404.

Knesel, K.M., Souza, Z.S., Vasconcelos, P.M., Cohen, B.E., Silveira, F.V., 2011. Young volcanism in the Borborema Province, NE Brazil, shows no evidence for a trace of the Fernando de Noronha plume on the continent. Earth and Planetary Science Letters 302, 38–50.

Laske, G., Masters, G., Ma, Z., Pasyanos, M., 2013. Update on CRUST1.0 - A 1-degree global model of Earth's crust. Geophysical Research Abstracts, 15, Abstract EGU2013-2658 .

Lavier, L.L., Steckler, M.S., Brigaud, F., 2001. Climatic and tectonic controls on the Cenozoic evolution of the West African margin. Marine Geology 178, 63–80.

Lithgow-Bertelloni, C., Silver, P.G., 1998. Dynamic topography, plate driving forces and the African superswell. Nature 395, 269–272.

Liu, S., Tommasi, A., Vauchez, A., Mazzucchelli, M., 2019. Crust-mantle coupling during continental convergence and break-up: Constraints from peridotite xenoliths from the Borborema Province, northeast Brazil. Tectonophysics 766, 249–269.

Lopes, R.P., 2002. O vulcanismo do arquipélago de Fernando de Noronha, PE: química mineral e geoquímica. Phd dissertation. Sao Paolo.

Lopes, R.P., Ulbrich, M.N.C., 2015. Geochemistry of the alkaline volcanic-subvolcanic rocks of the Fernando de Noronha Archipelago, southern Atlantic Ocean. Brazilian Journal of Geology 45, 307–333.

Lucazeau, F., 2019. Analysis and mapping of an updated terrestrial heat flow dataset. Geochemistry, Geophysics, Geosystems 20.

Marzoli, A., Melluso, L., Morra, V., Renne, P.R., Sgrosso, I., D'Antonio, M., Duarte Morais, L., Morais, E.A.A., Ricci, G., 1999. Geochronology and petrology of Cretaceous basaltic magmatism in the Kwanza basin (western Angola), and relationships with the Parana-Etendeka continental flood basalt province. Journal of Geodynamics 28, 341–356.

Mather, K.A., Pearson, D.G., McKenzie, D., Kjarsgaard, B.A., Priestley, K., 2011. Constraints on the depth and thermal history of cratonic

lithosphere from peridotite xenoliths, xenocrysts and seismology. Lithos 125, 729–742.

McKenzie, D., O'Nions, R.K., 1991. Partial melt distributions from inversion of rare earth element concentrations. Journal of Petrology 32, 1021–1091.

Morais Neto, J.M., Hegarty, K.A., Karner, G.D., Alkmim, F.F., 2009. Timing and mechanisms for the generation and modification of the anomalous topography of the Borborema Province, northeastern Brazil. Marine and Petroleum Geology 26, 1070–1086.

Moucha, R., Forte, A.M., Mitrovica, J.X., Rowley, D.B., Quéré, S., Simmons, N.A., Grand, S.P., 2008. Dynamic topography and long-term sea-level variations: There is no such thing as a stable continental platform. Earth and Planetary Science Letters 271, 101–108.

Ngonge, E.D., Hollanda, M.H.B.M., Pimentel, M.M., Oliveira, D.C., 2016. Petrology of the alkaline rocks of the Macau Volcanic Field, NE Brazil. Lithos 266-267, 453–470.

Nimis, P., Grütter, H., 2010. Internally consistent geothermometers for garnet peridotites and pyroxenites. Contributions to Mineralogy and Petrology 159, 411–427.

Nimis, P., Taylor, W.R., 2000. Single clinopyroxene thermobarometry for garnet peridotites. Part I. Calibration and testing of a Cr-in-Cpx barometer and an enstatite-in-Cpx thermometer. Contributions to Mineralogy and Petrology 139, 541–554.

O'Malley, C., White, N., Stephenson, S., Roberts, G., under review. Large-scale tectonic forcing of the African landscape and its drainage patterns. Journal of Geophysical Research: Earth Surface .

Perlingeiro, G., Vasconcelos, P.M., Knesel, K.M., Thiede, D.S., Cordani, U.G., 2013. $^{40}Ar/^{39}Ar$ geochronology of the Fernando de Noronha Archipelago and implications for the origin of alkaline volcanism in the NE Brazil. Journal of Volcanology and Geothermal Research 249, 140–154.

Pessoa Neto, O.d.C., Soares, U.M., Fernandes Da Silva, J.G., Roesner, E.H., Florencio, C.P., Valentin De Souza, C.A., 2007. Bacia Potiguar. Boletim de Geociências da Petrobras 15, 357–369.

Pinheiro, A.G., Julià, J., 2014. Normal thickness of the upper mantle transition zone in NE Brazil does not favour mantle plumes as origin for intraplate Cenozoic volcanism. Geophysical Journal International 199, 996–1005.

Pivin, M., Féménias, O., Demaiffe, D., 2009. Metasomatic mantle origin for Mbuji-Mayi and Kundelungu garnet and clinopyroxene megacrysts (Democratic Republic of Congo). Lithos 112, 951–960.

Priestley, K., McKenzie, D., 2006. The thermal structure of the lithosphere from shear wave velocities. Earth and Planetary Science Letters 244, 285–301.

Richards, F.D., Hoggard, M.J., White, N.J., Ghelichkhan, S., under review. Exploring the relationship between upper mantle structure and short wavelength dynamic topography using calibrated anelasticity parameterizations. Journal of Geophysical Research: Solid Earth .

Rivalenti, G., Mazzucchelli, M., Girardi, V.A., Vannucci, R., Barbieri, M.A., Zanetti, A., Goldstein, S.L., 2000. Composition and processes of the mantle lithosphere in northeastern Brazil and Fernando de Noronha: Evidence from mantle xenoliths. Contributions to Mineralogy and Petrology 138, 308–325.

Rivalenti, G., Zanetti, A., Girardi, V.A., Mazzucchelli, M., Tassinari, C.C., Bertotto, G.W., 2007. The effect of the Fernando de Noronha plume on the mantle lithosphere in north-eastern Brazil. Lithos 94, 111–131.

Roberts, G.G., White, N., 2010. Estimating uplift rate histories from river profiles using African examples. Journal of Geophysical Research 115, 1–24.

Robles-Cruz, S.E., Escayola, M., Jackson, S., Galí, S., Pervov, V., Watangua, M., Gonçalves, A., Melgarejo, J.C., 2012. U–Pb SHRIMP geochronology of zircon from the Catoca kimberlite, Angola: Implications for diamond exploration. Chemical Geology 310-311, 137–147.

Rodríguez Tribaldos, V., White, N.J., Roberts, G.G., Hoggard, M.J., 2017. Spatial and temporal uplift history of South America from calibrated drainage analysis. Geochemistry, Geophysics, Geosystems 18, 2321–2353.

Sahagian, D.L., 1988. Epeirogenic motions of Africa as inferred from Cretaceous shoreline deposits. Tectonics 7, 125–138.

Schaeffer, A.J., Lebedev, S., 2013. Global shear speed structure of the upper mantle and transition zone. Geophysical Journal International 194, 417–449.

Sial, A.N., Long, L., Pessoa, D., Kawashita, K., 1981. Potassium-argon ages and strontium isotope geochemistry of Mesozoic and Tertiary basaltic rocks, northeastern Brazil. Anais da Academia Brasileira de Ciências 53, 115–122.

Silveira, F.V., 2006. Magmatismo cenozóico da porção central do Rio Grande do Norte, NE do Brasil. Ph.D. thesis. Universidade Federal do Rio Grande do Norte.

Simões Neto, F.L., Julià, J., Schimmel, M., 2018. Upper-mantle structure of the Borborema Province, NE Brazil, from P-wave tomography: implications for rheology and volcanism. Geophysical Journal International 216, 231–250.

Souza, Z.S., Leite do Nascimento, M.A., Barbosa, R.V.N., Silveira Dias, L.G., 2005. Geology and tectonics of the Boa Vista Basin (Paraíba, northeastern Brazil) and geochemistry of associated Cenozoic tholeiitic magmatism. Journal of South American Earth Sciences 18, 391–405.

Steinberger, B., 2016. Topography caused by mantle density variations: Observation-based estimates and models derived from tomography and lithosphere thickness. Geophysical Journal International 205, 604–621.

Sykes, L.R., 1978. Intraplate seismicity, reactivation of preexisting zones of weakness, alkaline magmatism, and other tectonism postdating continental fragmentation. Reviews of Geophysics and Space Physics 16, 621–688.

Tainton, K.M., McKenzie, D., 1994. The generation of kimberlites, lamproites, and their source rocks. Journal of Petrology 35, 787–817.

Torquato, J., Amaral, G., 1973. Algumas idades K/Ar do magmatismo mesozóico de Angola e sua correlação com o correspondente do sul do Brasil. Boletim do Instituto de Investigação Científica de Angola 10, 31–38.

Walker, R.T., Telfer, M., Kahle, R.L., Dee, M.W., Kahle, B., Schwenninger, J.L., Sloan, R.A., Watts, A.B., 2016. Rapid mantle-driven uplift along the Angolan margin in the late Quaternary. Nature Geoscience 9, 909–914.

Yamauchi, H., Takei, Y., 2016. Polycrystal anelasticity at near-solidus temperatures. Journal of Geophysical Research: Solid Earth 121, 7790–7820.

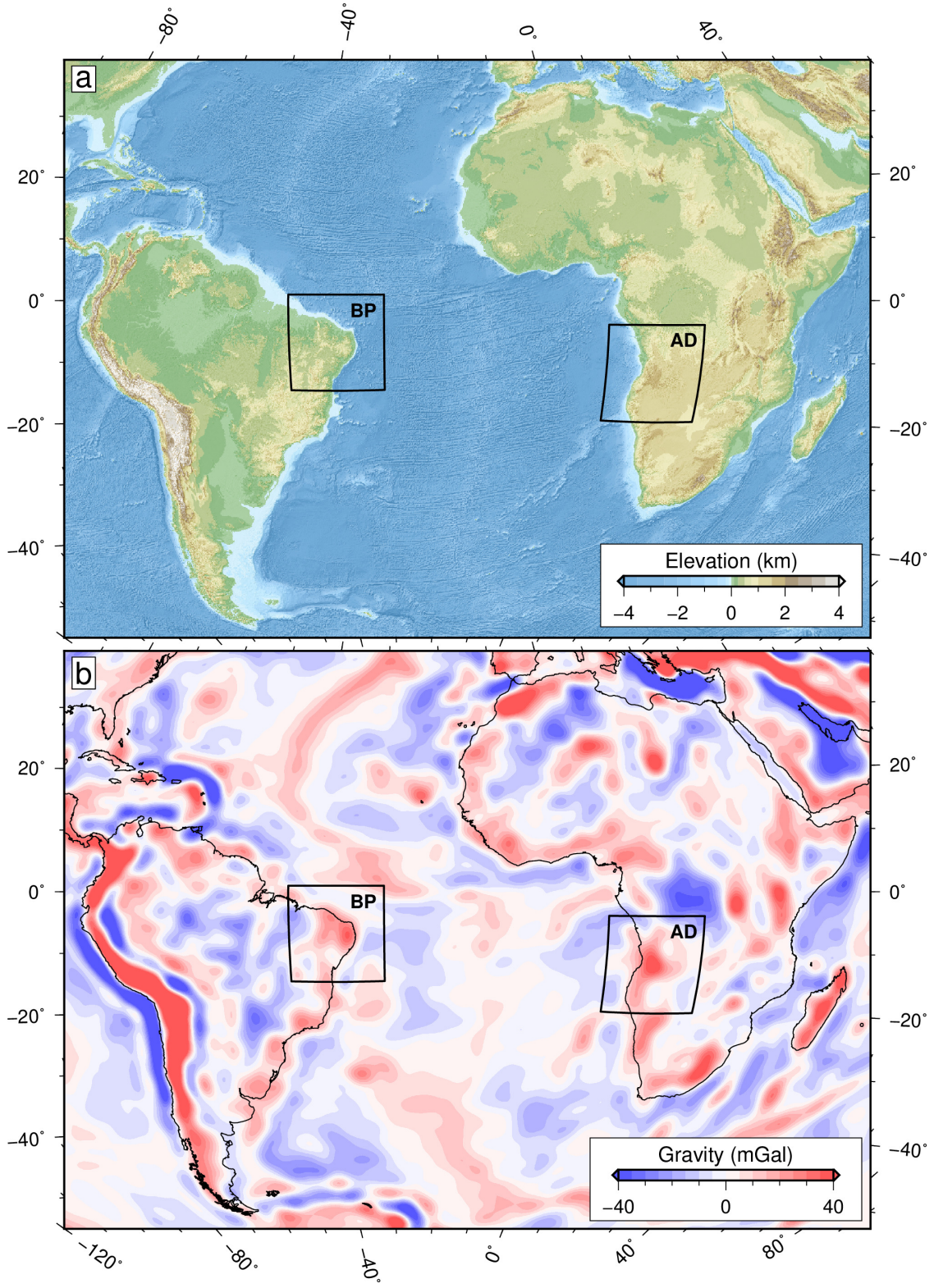

Figure 1: (**a**) Elevation and bathymetry of South Atlantic region. Black boxes = prominent topographic domes in northeast Brazil (BP; Borborema Province) and southwest Africa (AD; Angolan dome). (**b**) Satellite-derived free-air gravity anomalies bandpass-filtered between 500–4000 km (Bruinsma et al., 2014).

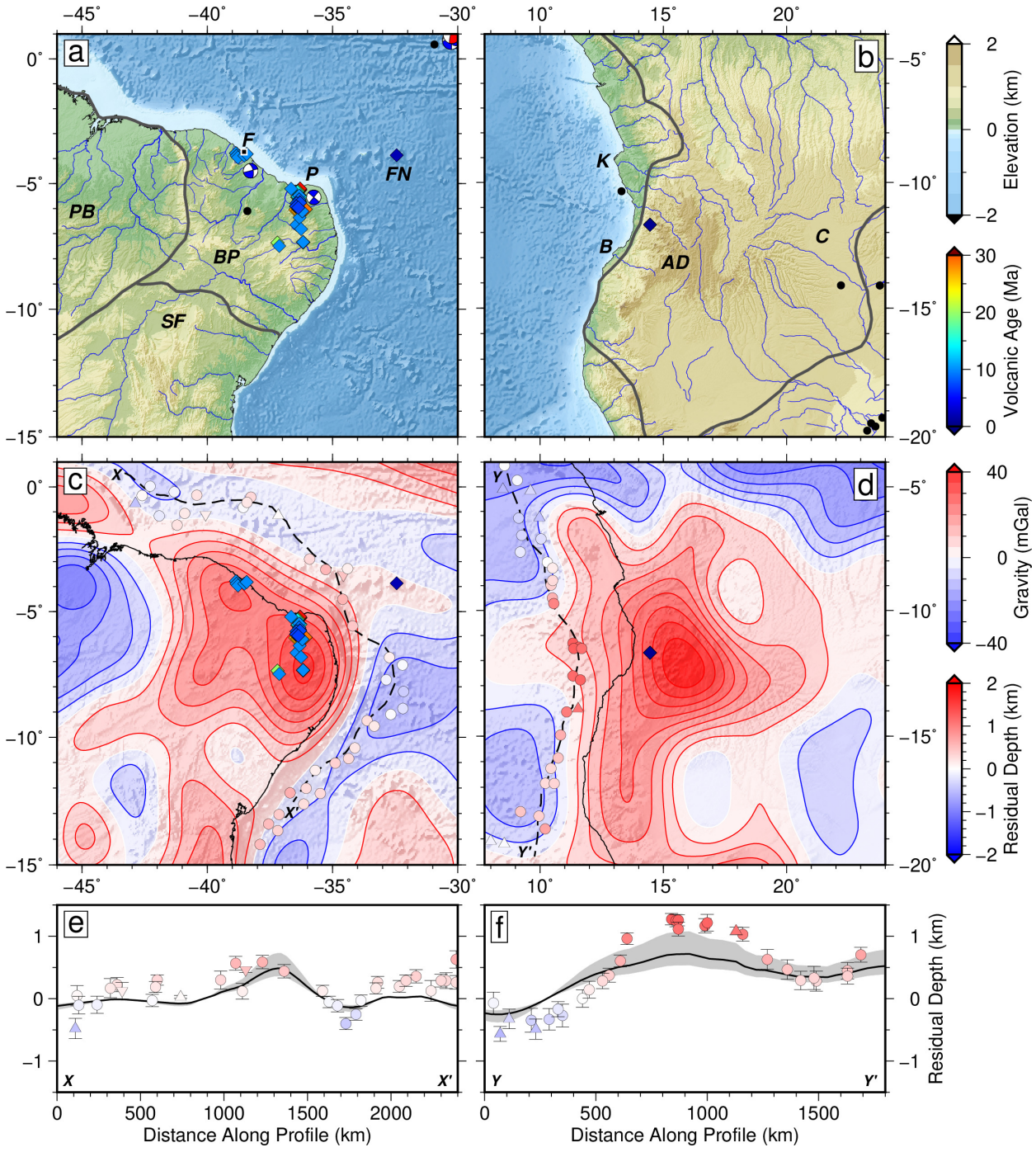

Figure 2: (**a**) Topographic map of northeast Brazil. Blue lines = drainage network; black circles = earthquakes of M_w < 5; beachballs = focal mechanisms for earthquakes of M_w > 5; diamonds = volcanic activity < 50 Ma, coloured by age; grey lines = province boundaries; BP = Borborema Province; F = Fortaleza; FN = Fernando de Noronha; P = Potiguar basin; PB = Parnaíba basin; SF = São Francisco craton. (**b**) Same for southwest Africa. AD = Angolan dome; B = Benguela basin; C = Congo craton; K = Kwanza basin. (**c**) Free-air gravity anomalies in northeast Brazil, bandpass-filtered between 500–4000 km (Bruinsma et al., 2014). Coloured circles and up/downward triangles = accurate estimates and lower/upper bounds of oceanic residual depth anomalies (Hoggard et al., 2017); dashed line = transect shown in (e). (**d**) Same for southwest Africa; dashed line = transect shown in (f). (**e**) North-to-south transect offshore Brazil of residual depths within a corridor of 80 km ± 1σ. Black line with grey band = free-air gravity anomalies scaled using admittance, $Z = 30 \pm 10$ mGal km^{-1}. (**f**) Same as (e) for southwest Africa.

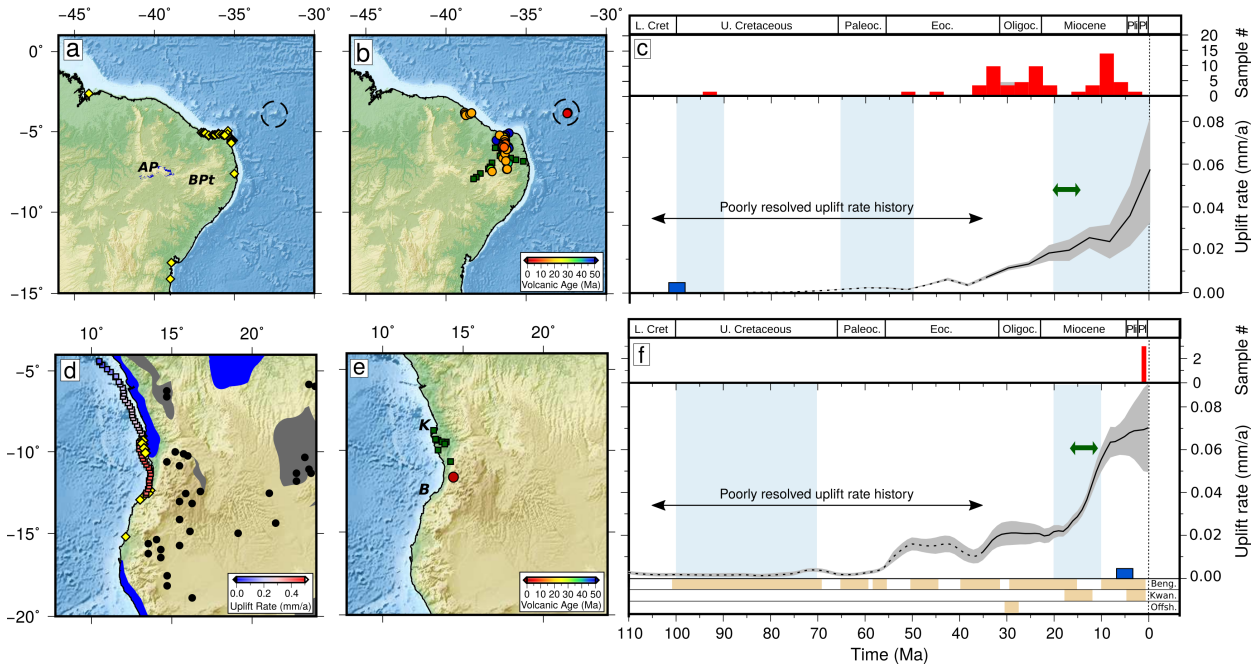

Figure 3: Uplift histories derived from river inverse modelling. (**a**) Topographic map of northeast Brazil. Yellow diamonds = uplifted Oligo-Miocene coastal deposits and Holocene marine terraces (Bezerra et al., 2003; CPRM-Serviço Geológico do Brasil, 2004); blue polygons = shallow marine limestones of the Albian Santana Formation (Arai, 2014); AP = Araripe Plateau; BPt = Borborema Plateau. (**b**) Coloured circles = volcanic activity < 50 Ma, coloured by age; green squares = location of apatite fission track analysis (Morais Neto et al., 2009). (**c**) Black line with grey band = uplift rate history with $\pm 1\sigma$ for nodes located at the centre of the Borborema Province; histogram = magmatic samples (red bars = $^{40}Ar/^{39}Ar$ ages, grey bars = K-Ar ages); vertical blue bars = exhumation events from thermochronology studies; dark blue box = timing of deposition of youngest marine sedimentary rocks (Santana Formation); green arrow = onset of increased clastic deposition input into offshore basins (Córdoba et al., 2007; Pessoa Neto et al., 2007). Panels (a–c) modified from (Rodríguez Tribaldos et al., 2017). (**d**) Topographic map of southwest Africa. Blue polygons = distribution of Cenomanian marine sedimentary rocks (Sahagian, 1988); black circles = indurated laterite deposits during Paleogene times (Burke and Gunnell, 2008); grey polygons = distribution of lateritic gravel deposits; yellow diamonds = uplifted Pleistocene marine terraces (Guiraud et al., 2010); blue to red squares = location of uplift rate estimates derived from seismic reflection stacking velocities (Al-Hajri et al., 2009; Hoggard et al., 2017). (**e**) Red circle = volcanic activity < 50 Ma, coloured by age; green squares = location of apatite fission track analysis (Jackson et al., 2005). K = Kwanza; B = Benguela. (f) Black line with grey band = uplift rate history with $\pm 1\sigma$ for nodes located at the centre of the Angolan dome from O'Malley et al. (under review). Histogram = magmatic samples; vertical blue bars = exhumation events from thermochronology studies; dark blue box = timing of deposition of youngest marine sedimentary rocks; green arrow = onset of increased clastic deposition input into offshore Kwanza basin (Lavier et al., 2001; Jackson et al., 2005; Al-Hajri et al., 2009); bottom orange bands = times of sedimentation hiatus and erosional unconformity development (Jackson et al., 2005; Guiraud et al., 2010; Al-Hajri et al., 2009).

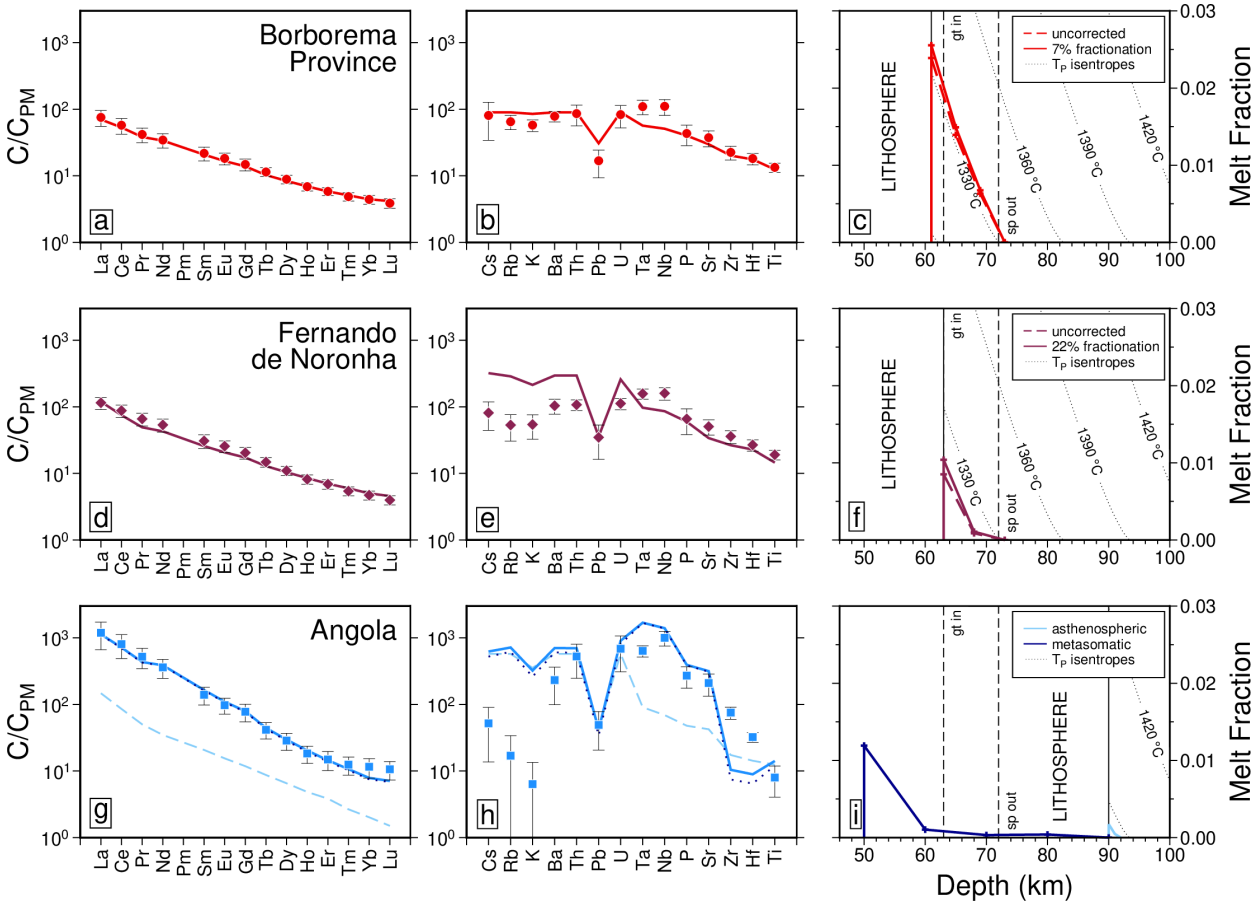

Figure 4: REE inverse modelling of 56 samples from Borborema Province, 34 samples from Fernando de Noronha, and 10 samples from Angola. (**a**) Rare earth element (REE) concentrations for samples from Borborema Province normalised to primitive mantle (PM) (McKenzie and O'Nions, 1991). Red circles with vertical bars = mean concentrations ± 1σ; red line = best-fit concentrations calculated by inverse modelling. (**b**) Trace element concentrations for Borborema Province. Red line = prediction from forward modelling of optimal melting model. (**c**) Melt fraction as function of depth. Solid red line = melt fraction (corrected for 7% olivine fractionation) obtained by fitting average REE composition shown in (a); dashed red line = uncorrected melt fraction; dotted lines = isentropic melting curves labelled according to potential temperature, T_P; vertical dashed lines = phase boundaries for spinel and garnet. (**d–f**) Same for Fernando de Noronha, corrected for 22% olivine fractionation. (**g–i**) Same for Catanda volcanics in Angola, where best-fitting composition is a mixture of asthenospheric (light blue) and metasomatic (dark blue) melts.

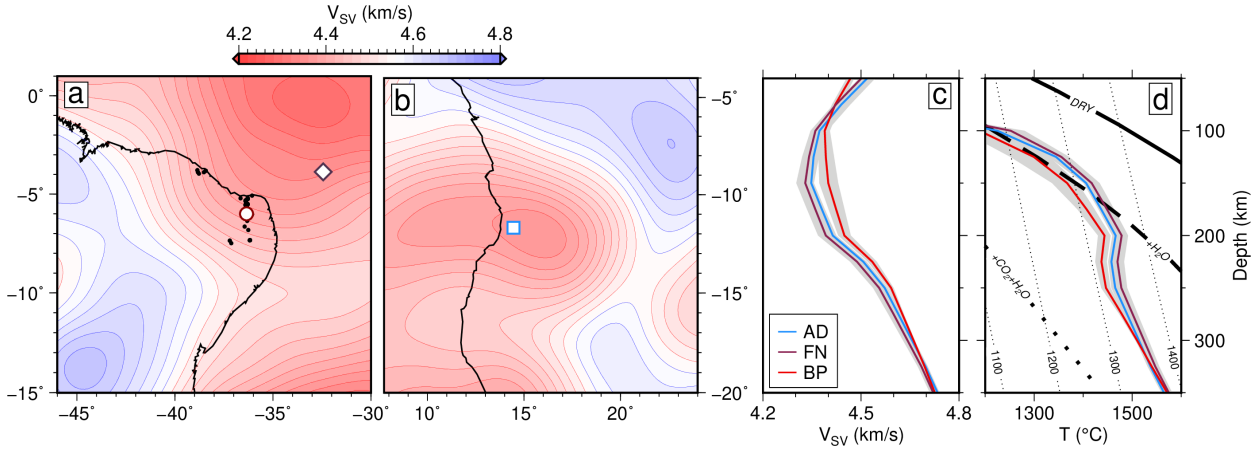

Figure 5: (**a**) Average shear wave velocity over 100–200 km depth range for northeast Brazil from SA2019 tomography model (Celli et al., 2020). Black circles = volcanic activity < 50 Ma; white symbols = loci of velocity profiles shown in panel (c). (**b**) Same for southwest Africa. (**c**) Shear wave velocity, V_{SV}, as function of depth for Brazilian and African locations shown in panels (a–d). Blue line = Angola (AD); purple line = Fernando de Noronha (FN); red line = Borborema Province (BP); grey envelope = variation within 1° radius around profile locations; coarse dashed line = reference model. (**d**) Temperature as function of depth calculated from V_{SV} profiles shown in panel (c). Colour scheme as before. Thick solid diagonal line = dry peridotite solidus; thick dashed diagonal line = peridotite solidus in presence of 0.1 wt% water (Katz et al., 2003); dotted diagonal line = peridotite solidus in presence of 0.5 wt% water and 3 wt% CO_2 (Foley et al., 2009); thin dashed lines = mantle isentropes labelled according to potential temperature, T_P.

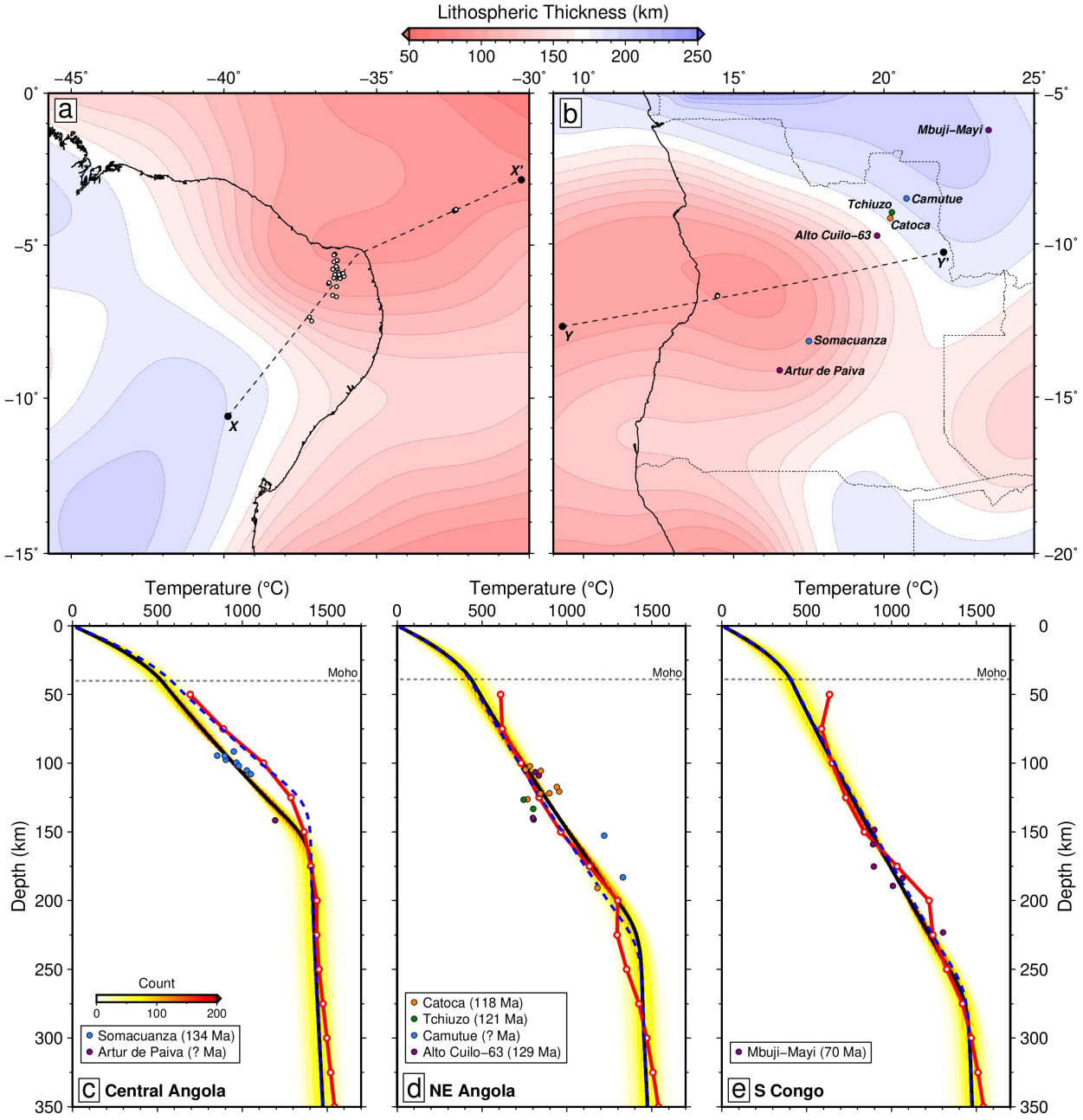

Figure 6: (**a**) Present-day lithospheric thickness beneath northeast Brazil, calculated by converting the SA2019 seismic tomography model to temperature and mapping the 1175 °C isotherm (Celli et al., 2020; Hoggard et al., 2020; Richards et al., under review). White circles = volcanic samples analysed in this study; black dashed line = location of transect in Figure 7. (**b**) Same for Angola; coloured circles = kimberlite pipes containing mantle xenocrysts. (**c**) Thermobarometry for central Angola; circles = xenocryst P-T estimates; dashed line = Moho; black line/yellow band = palaeogeotherm and uncertainty derived from FITPLOT modelling (Mather et al., 2011; Hoggard et al., 2020); red line = present-day temperatures obtained from tomography; blue dashed line = present-day geotherm using FITPLOT on tomographically-derived temperature profile. Note lithospheric thinning by ~ 30 km. (**d**) Same for northeast Angola. (**e**) Same for southern Congo.

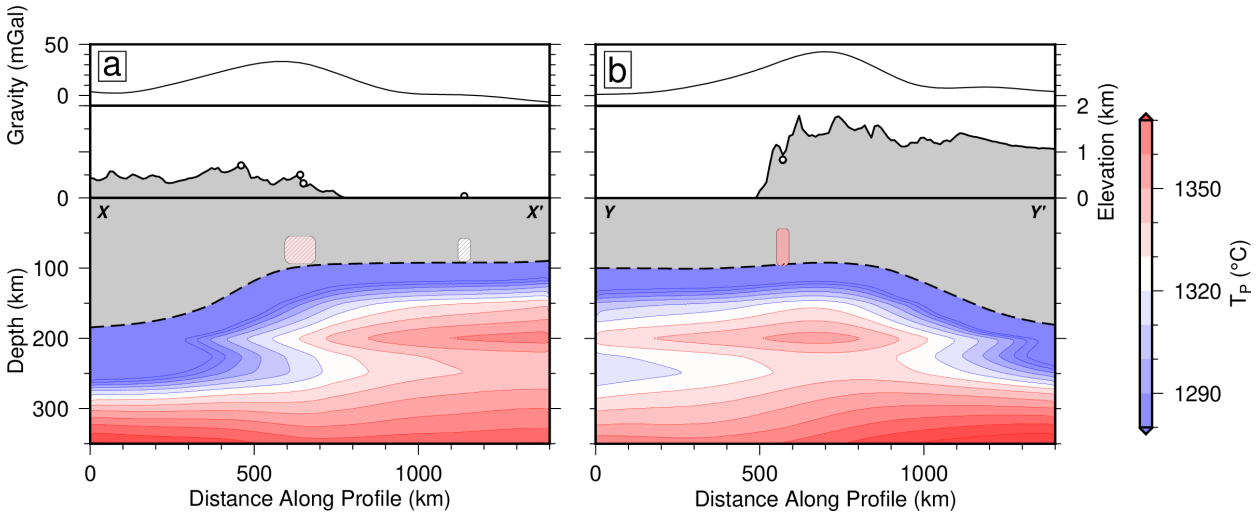

Figure 7: (**a**) Transect of gravity, topography and mantle structure for northeast Brazil (location in Figure 6a). Thin black line = satellite-derived free-air gravity anomaly, bandpass-filtered between 500–4000 km (Bruinsma et al., 2014); grey polygon = lithosphere; dashed line = lithospheric thickness calculated from SA2019 tomography model; coloured grid = potential temperature (T_P) calculated from SA2019 tomography model; white circles = volcanic rocks within 10 km of transect; hashed polygons = melting region inferred from volcanic geochemistry, coloured by geochemically inferred maximum T_P. (**b**) Same for southwest Africa (location in Figure 6b.)